Available online at www.sciencedirect.com

ScienceDirect

Geochimica et Cosmochimica Acta 142 (2014) 115–131

Geochimica et Cosmochimica Acta

www.elsevier.com/locate/gca

Isotopic diversity in interplanetary dust particles and preservation of extreme ^{16}O-depletion

N.A. Starkey [a,*], I.A. Franchi [a], M.R. Lee [b]

[a] Planetary and Space Sciences, The Open University, Walton Hall, Milton Keynes MK7 6AA, UK
[b] School of Geographical and Earth Sciences, University of Glasgow, Gregory Building, Lilybank Gardens, Glasgow G12 8QQ, UK

Received 4 March 2014; accepted in revised form 12 July 2014; available online 27 July 2014

Abstract

Two interplanetary dust particles (IDPs) investigated by NanoSIMS reveal diverse oxygen isotope compositions at the micrometre-scale. The oxygen isotope values recorded at different locations across the single IDP fragments cover a wider range than the bulk values available from all IDPs and bulk meteorites measured to date. Measurement of H, C, and N isotopes by NanoSIMS, and the use of scanning and transmission electron microscopy (SEM and TEM) to determine elemental compositions and textural information allows for a better understanding of the lithologies and organic signatures associated with the oxygen isotope features.

IDP Balmoral, a ~15 μm-sized fragment with a chondritic porous (CP)-IDP-like texture, contains a region a few micrometres in size characterised by ^{16}O-depleted isotope signatures in the range $\delta^{17}O$, $\delta^{18}O = +80‰$ to $+200‰$. The remainder of the fragment has a more ^{16}O-rich composition ($\delta^{18}O = 0–20‰$), similar to many other IDPs and bulk meteorites. Other than in discrete pre-solar grains, such extreme ^{16}O-depletions have only been observed previously in rare components within the matrix of the Acfer 094 meteorite. However, TEM imaging and FeO/MgO/Si ion ratios indicate that the ^{16}O-depleted regions in Balmoral did not form by the same mechanism as that proposed for the ^{16}O-depleted phases in Acfer 094. As the level of ^{16}O depletion is consistent with that expected from isotope selective self-shielding, it is likely that the ^{16}O-depleted reservoir was located close to that where oxygen self-shielding effects were most pronounced (i.e., the outer solar nebula or even interstellar medium).

Individual regions within IDP Lumley cover a range in $\delta^{18}O$ from $-30‰$ to $+19‰$, with the oxygen isotope values broadly co-varying with δD, $\delta^{13}C$, $\delta^{15}N$, light-element ratios and texture. The relationships observed in Lumley indicate that the parent body incorporated material at the micrometre-scale from discrete diverse isotopic reservoirs, some of which are represented by inner Solar System material but others which must have formed in the outer Solar System.

The IDP fragments support a model whereby primary dust from the early solar nebula initially formed a variety of reservoirs in the outer solar nebula, with those at lower AU incorporating a higher proportion of inner Solar System chondritic dust than those at larger AU. These reservoirs were subsequently disrupted into micrometre-sized clasts that were re-incorporated into IDP parent bodies, presumably at large AU. These results reveal that any models accounting for mixing processes in the early solar nebula must also account for the presence of an extremely ^{16}O-depleted reservoir in the comet-forming region.

1. INTRODUCTION

Interplanetary dust particles (IDPs) originate from comets and asteroids and can be collected by aircraft in the

* Corresponding author. Tel.: +44 (0)1908 858847.
E-mail address: natalie.starkey@open.ac.uk (N.A. Starkey).

http://dx.doi.org/10.1016/j.gca.2014.07.011
0016-7037/

Earth's stratosphere. However, despite some dedicated collections that coincide with particular meteor showers (Messenger, 2002; Busemann et al., 2009; Bastien et al., 2013), it is unknown from which parent body an individual IDP originates. Dynamical modelling of dust ejected from comets and asteroids indicates that over 85% of the total mass influx of dust to the Earth originates from Jupiter-family comets (JFCs) (Nesvorny et al., 2010). Samples of comets should retain the best preserved components of the Solar System starting materials because they formed at large heliocentric distances of 5–30 AU, where temperatures, at their most extreme, reach down to ~30 K (Bockelée-Morvan et al., 2005). Furthermore, IDPs have remained locked in ice at low temperatures until their release from the cometary surface not long before arrival at the top of the Earth's atmosphere. Laboratory analysis of IDPs has revealed their primitive nature, such as high abundances of presolar grains (Messenger et al., 2003; Floss et al., 2006; Busemann et al., 2009; Davidson et al., 2012), the presence of GEMS (Glass with Embedded Metal and Sulphides; Bradley, 1994; Keller and Messenger, 2011) and an abundance of primitive carbonaceous material (Messenger, 2000; Floss et al., 2006; Busemann et al., 2009; Matrajt et al., 2012; Starkey et al., 2013). These primitive features suggest it is likely that IDPs provide access to samples of the early Solar System from bodies that are otherwise hard to access from Earth, and which may never have been sampled by meteorites, or survived the aqueous and/or thermal alteration processes experienced by meteoritic material on parent asteroids.

IDPs are composed of a complex mix of silicate and organic material that forms a wide range of particle textures. To understand the earliest-formed material in the Solar System it is the finest-grained IDPs that are likely to contain the most primitive material as their texture is similar to that expected for direct condensates from the solar nebula. However, the origin of individual components within fine-grained IDPs can also clearly be extra solar (i.e., existence of presolar grains). IDPs also contain abundant fine-grained amorphous siliceous material and primitive carbonaceous matter. The origin of amorphous silicates in IDPs, such as GEMS, is very much debated, with some models suggesting that the majority form in the solar nebula as late-stage non-equilibrium condensates (e.g., Keller and Messenger, 2011), while others prefer formation in the interstellar medium (e.g., Bradley, 1994). In many cases, large (up to several micrometres) crystalline silicate mineral fragments are contained within the ultra-fine-grained IDPs. Such minerals require a high-temperature formation environment and are likely to have originated in the hot inner Solar System, which is supported by their chondritic-like O isotope compositions ($\delta^{18}O = \sim 0‰$) (Aleon et al., 2009; Nakashima et al., 2012). The presence in IDPs of minerals that crystallised at high temperatures can be accounted for by transport of such material from the inner Solar System out to large AU in relatively short timescales by turbulent radial mixing (Bockelée-Morvan et al., 2002; Ciesla, 2007). Such transport has been suggested in order to account for the presence of high-temperature minerals in the Wild2 samples collected by Stardust (Nakamura et al., 2008; Simon et al., 2008). Therefore, analysis of these mineral fragments, or of the bulk composition of IDPs containing such material, will not provide information about the composition of the outer solar nebula.

Only a small number of fine-grained IDPs have been measured for bulk O isotopes at a level of precision that is high enough for their comparison to meteorites (Engrand et al., 1999; Aleon et al., 2009; Snead et al., 2012; Starkey and Franchi, 2013). These analyses have shown that IDPs cover a wider range of O isotope values than that displayed by bulk meteorites, from relatively ^{16}O-rich values of $\delta^{18}O \approx -20‰$, to ^{16}O-poor, chondritic-like values of $\delta^{18}O = 0‰$ to $+20‰$ (Aleon et al., 2009; Starkey and Franchi, 2013). Such large isotopic variations appear to reflect the wide range of parent body sources sampled by IDPs. These parent bodies presumably cover a range from primitive asteroids and comets that preserve, in part, the signature of original solar nebula dust, to parent bodies that are dominated by material processed in the inner Solar System (Starkey and Franchi, 2013). However, considering the extremely fine-grained texture of IDPs, and the potential for them to have incorporated fine-grained material from a wide portion of the early solar nebula, it is paramount to investigate IDPs at the micrometre-scale to understand the reservoirs they have sampled and the nature of the transportation and mixing processes that created the components. Very few detailed O isotopic studies have been made of multiple fragments from single cluster IDPs. The limited data set available shows that fragments from any one cluster IDP produce results within error of each other, suggesting some level of O isotopic homogeneity within a single IDP parent body (Starkey and Franchi, 2013). This could reflect a limited number of different components being available, efficient mixing at all scales prior to accretion, and/or homogenisation of components. Considerable expansion of the IDP data is required to assess the importance of these different processes. It is also important to analyse ultrafine- to fine-grained IDPs as these materials are more likely to not have been processed close to the Sun, as opposed to larger mineral fragments that may represent high-temperature components formed in the inner Solar System.

H, C and N isotopes in IDPs can show substantial isotopic variations at the micrometre-scale (Messenger, 2000; Aleon et al., 2001; Floss et al., 2006; Busemann et al., 2009). These isotopic variations normally reflect the presence of carbonaceous material with isotopically anomalous compositions (Floss et al., 2006, 2011) indicating the potential survival of molecular cloud (Messenger, 2000) or cold outer disk (Remusat et al., 2009) material. In addition, extreme isotopic anomalies at the sub-micrometre scale can also be due to the presence of presolar grains carrying isotopic signatures of nucleosynthetic events. Although C and N isotopic anomalies within single IDPs are sometimes related, H isotope anomalies have not been observed to follow the same pattern (Floss et al., 2006). Studies that relate the bulk H, C and N isotope signatures with bulk O isotopes in the same IDP samples are of paramount importance for understanding how the silicate and organic reservoirs that contributed to these primitive materials may be related.

This study focusses on fine-grained fragments from two IDP cluster particles obtained from the NASA Cosmic Dust Laboratory. The relatively large size of the fragments meant that it was possible to obtain multiple O isotope analyses across the single fragments to detail O isotope variations at the few-micrometre-scale in fine-grained materials, at a level of precision that was suitable for comparison to the meteorite record. In addition, it was possible to obtain corresponding H, C, and N isotopic compositions on the same areas analysed for O. In addition, TEM analysis of one of the fragments was undertaken post-NanoSIMS to assess the mineralogy of the isotopic anomalies identified.

2. METHODS

2.1. X-ray elemental analysis

An FEI Quanta 2003D DualBeam™ focused ion beam scanning electron microscope (FIB-SEM) fitted with an Oxford instruments 80 mm X-max energy dispersive X-ray detector (EDX) system was used at the Open University to perform EDX analyses at various locations on IDP fragments (see Electronic Annex). The same instrument was also used to obtain an electron-transparent section (~10 × 2 μm and ~100 nm thickness) of a ^{16}O-depleted region of Balmoral1 by FIB-lift-out post-NanoSIMS in order for the mineralogy to be investigated by transmission electron microscopy (TEM). Further details are available in the Electronic Annex.

2.2. X-ray imaging analysis

A Zeiss Supra 55V analytical field emission gun scanning electron microscope (FEG-SEM) at the Open University was used to obtain high resolution, high magnification secondary electron (SE) images (at 4 kV and 5 mm working distance) of the samples to assess particle texture.

2.3. NanoSIMS isotopic analyses

The NanoSIMS 50L at The Open University was used to obtain both O isotope spot and imaging and H, C, and N isotopic imaging analyses of single IDP fragments at a level of precision that allows for their comparison to the meteorite record.

The H, C and N isotope analyses were made prior to O isotope analyses. The protocol used follows that set out in Starkey and Franchi (2013) and is summarised here with some further details in the Electronic Annex. In all cases negative secondary ions were collected on electron multipliers with the first analytical set-up collecting ^{12}C, ^{13}C, ^{16}O, ^{12}C^{14}N, ^{12}C^{15}N and ^{28}Si simultaneously and the second analytical set-up collecting ^{1}H, ^{2}H and ^{12}C simultaneously for each particle. A Cs^+ probe with a current of 1.5 pA for C and N isotope measurements, and 3 pA for H isotope measurements was rastered over the sample with a raster size (and pre-sputter raster size) relevant to the particular area of fragment being analysed (usually around 10–15 μm for analysis). The probe size was typically ⩽150 nm and the raster were conducted with a pixel step of ⩽100 nm and a dwell time of 1000 μs per pixel. Charge compensation was applied with an electron gun with the same settings used on the sample and standard. Data were collected in planes with total analysis times of ≈40 min. Planes of image data were corrected for detector deadtime and sample drift, combined and processed using the Limage software (L. Nittler, Carnegie Institute of Washington) to provide bulk δ^{13}C, δ^{15}N, δD and C/H ratios for each fragment, as well as regions of interest (ROI) for the same areas as obtained in the O isotope analyses to provide complementary data. Further analytical details are available in Electronic Annex. H, C and N isotope results are reported as $\delta^{13}C_{PDB}$, $\delta^{15}N_{AIR}$ and δD_{SMOW}. All isotope ratio errors are reported as 2σ and include the external reproducibility from all standards analysed during the session (over several days) together with internal uncertainty from each IDP measurement. The standard used was IOM (insoluble organic matter; extracted by acid demineralisation of bulk meteorites (Alexander et al., 2007)) from the CM2 Cold Bokkeveld that was analysed immediately before and/or after each IDP.

IDPs were analysed in O isotope imaging mode prior to O isotope spot analyses. A Cs^+ ion beam of 2 pA was rastered across a 10 × 10 μm analysis areas (15 × 15 μm for pre-sputter), allowing for 3 image analyses on Lumley1 and one on Balmoral1. The instrument was set to a mass resolving power of >10,000 (Cameca NanoSIMS definition, based on the measured peak width containing 80% of the ion beam) primarily to resolve the interference of ^{16}OH on ^{17}O. The probe size was typically ⩽150 nm and the raster were conducted with a pixel step of ⩽100 nm and a dwell time of 1000 μs per pixel. Data were collected in 50 planes with auto-centring of the peak positions every 10 frames. Charge compensation was applied with an electron gun with the same settings used on the sample and standard. Secondary ions of ^{16}O, ^{17}O and ^{18}O were collected simultaneously on electron multipliers along with ^{28}Si, ^{24}Mg^{16}O and ^{40}Ca^{16}O. Total counts of ^{16}O for the mapped areas were ~1 × 10^9. Standard analyses in imaging mode were performed on flat, polished San Carlos olivine crystals on comparably-sized areas to the IDP fragment analyses. Similar analyses on flat, polished Eagle Station olivine calibrated against San Carlos Olivine gave correct values within error of the true value as measured by laser fluorination (Starkey and Franchi, 2013). Results from smaller regions of interest within the images were processed using the Limage software and corrected for position drift, detector dead time and quasi-simultaneous arrival (QSA) effect.

Oxygen isotope spot analyses were obtained following the protocol described in Starkey and Franchi (2013) and summarised here with further details in the Electronic Annex. In spot mode, a Cs^+ ion beam with a 25 pA current was rastered over 5 × 5 μm analysis areas (7 × 7 μm area for pre-sputtering with a 50 pA probe). The instrument was set to the same mass resolving power conditions as for the O image analyses. In spot mode, secondary ions of ^{16}O were collected on a faraday cup while secondary ions of ^{17}O and ^{18}O were collected simultaneously on electron multipliers. Total counts of ^{16}O for the spot analyses were

on the order of $\sim 4 \times 10^9$. Charge compensation was applied with an electron gun with the same settings on the sample and standard. Isotope ratios were normalised to Standard Mean Ocean Water (SMOW) using a San Carlos olivine standard that bracketed the sample analyses in order to generate $\delta^{17}O$ and $\delta^{18}O$ values and also to provide corrections for instrumental mass fractionation.

All errors for O isotope analyses, whether spot or imaging mode, are given as 2 sigma which combines internal errors for each analysis with the standard deviation of the mean of the associated standard. Errors are, on the whole, larger for imaging analyses due to poorer counting statistics because of the smaller probe size required to measure ^{16}O on an electron multiplier.

2.4. High resolution transmission electron microscopy

High resolution transmission electron microscope (HR-TEM) imaging of the FIB-produced section from Balmoral1 was carried out at The Open University on a JEOL JEM 2100 equipped with a lanthanum hexaboride (LaB_6) emitter operating at 200 kV. Images were captured using an Orius SC1000 digital camera from Gatan at column magnifications up to ×250,000.

The Balmoral1 FIB-lift-out section was also examined at the University of Glasgow by low voltage scanning transmission electron microscopy (LV-STEM) using a Zeiss Sigma field-emission SEM operated at 20 kV/1 nA and following the procedures of Lee and Smith (2006). LV-STEM enabled the acquisition of bright-field and annular dark-field images, and chemical analyses were obtained using an Oxford Instruments X-Max silicon-drift X-ray detector operated through INCA software. All of these analyses have X-rays contributed from Al from the STEM holder and/or the substrate surrounding the IDP fragment, and many also contain Cu from the grid onto which the foil was welded, and from Pt that was deposited prior to FIB milling.

Following LV-STEM work, selected area electron diffraction (SAED) patterns were obtained from the FIB-section using a FEI T20 TEM at the University of Glasgow operated at 200 kV. All SAED patterns were acquired using a ~200 nm diameter aperture, and manually indexed. The smallest grains that could be identified by SAED were ~50 nm across.

3. RESULTS

3.1. Sample description

Two individual fragments were obtained from IDP cluster particle 10 on collector L2009 and are named hereafter Lumley1 (L2009-AA1; Fig. 1) and Lumley2 (L2009-Z1; Electronic Annex Figure A).

Lumley1 is large (25 × 30 μm) and irregularly shaped after pressing (Fig. 1). FEG-SEM imaging reveals that Lumley1 exhibits a variation in texture across the fragment, including large featureless, smooth/compact-looking regions up to 10 μm in size, fine-grained areas where the grains are ≪1 μm, and more coarse-grained areas where grains are observable in the ~1–2 μm range. EDX spectra reveal an approximately chondritic major elemental composition across various regions of the fragment (see Electronic Annex Figure A). C/H ratios obtained from NanoSIMS imaging reveal that the majority of Lumley1 has a C/H ⩾ 1 but the values can vary in different locations from C/H = 0.5–1.3 (see Electronic Annex). It should be noted that measuring C/H value by SIMS may not be the perfect technique because of differences in H ion emission from hydrous and organic phases. However, the results here are discussed within the context of the empirical observations by Aleon et al. (2001), the results of which have shown some consistency for IDPs in the study of Starkey and Franchi (2013). In these studies, a C/H > 1 is generally interpreted as indicating the anhydrous nature of an IDP (see Aleon et al., 2001 and Starkey and Franchi, 2013) suggesting that Lumley1 is composed predominantly of anhydrous material, but with some smaller hydrous areas.

The differences in C/H ratio and texture do not co-vary, and because of the large range in textures and C/H ratios it makes it hard to define Lumley1 as either chondritic-porous (CP-), even though it is predominantly anhydrous in C/H ratio, or chondritic-smooth (CS-). Three O isotope spots (with a size of 5 × 5 μm) and three O isotope maps (with sizes of 10 × 10 μm) were obtained across different areas of Lumley1. Complementary H, C and N isotope ratio maps were obtained for the same areas from 25 × 25 μm NanoSIMS isotopic maps in which ROIs were subsequently defined in the Limage software to correspond with the O isotope regions.

Lumley 2 is a slightly smaller fragment (12 × 20 μm in size) from the same cluster as Lumley1. The texture across Lumley2 is less variable compared to Lumley1, with it being composed predominantly of fine-grained material (grains < 1 μm) but with some areas that are more featureless in appearance. EDX spectra reveal an approximately chondritic elemental composition across most regions of the fragment, but in one location a small Fe-rich region is observed (see Electronic Annex Figure B). C/H ratios for Lumley2 vary from 0.9 to 1.0, which is similar to Lumley1 and suggests that the particle is largely anhydrous. One O isotope spot analysis and one O isotope map of the bulk particle was obtained on Lumley2. H, C and N isotopic data for Lumley2 were obtained in imaging mode but from a different region of the particle which had split up on pressing into gold (see Electronic Annex Figure B).

One individual fragment was obtained from the IDP cluster particle 2 of collector L2071 and is hereafter named Balmoral1 (L2071-H1). Once pressed into gold foil, Balmoral1 is approximately 12 × 16 μm in size with a fine-grained texture, composed of grains that appear in SEM imaging to be ≪1 μm (Fig. 2a), similar to the fine-grained texture of CP-IDPs. EDX spectra obtained from Balmoral1 are consistent with a chondritic composition (see Electronic Annex Figure C). The bulk fragment has a C/H = ~1 but there is a small region contained within the fragment with C/H < 1 and which will be discussed in more detail. One O isotope map of the bulk fragment was acquired prior to two O isotope spot analyses (5 × 5 μm spots) which were obtained at different ends of the

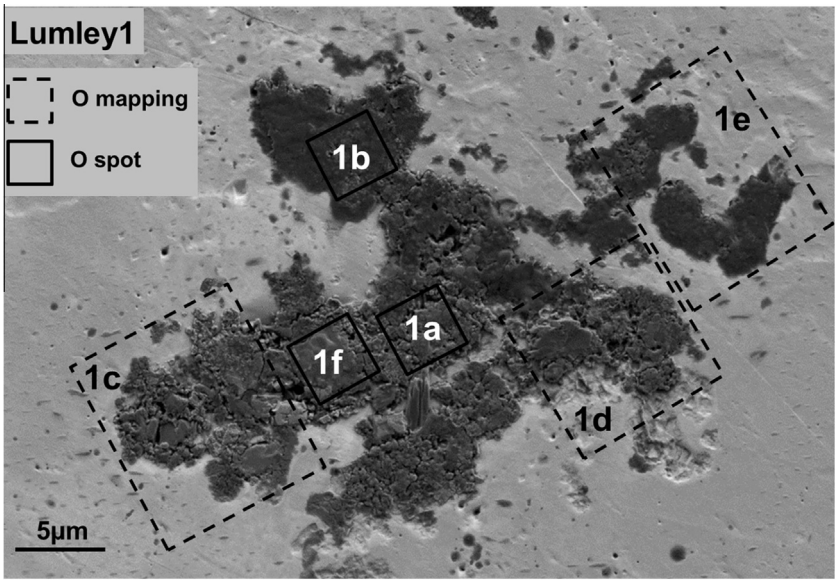

Fig. 1. Secondary electron image of IDP Lumley1 pressed flat into gold foil showing the variable texture across the fragment. Location of oxygen isotope analytical spots are marked with solid line and images with a dashed line. Labels 1a–1f correspond to Table 1 and Fig. 3.

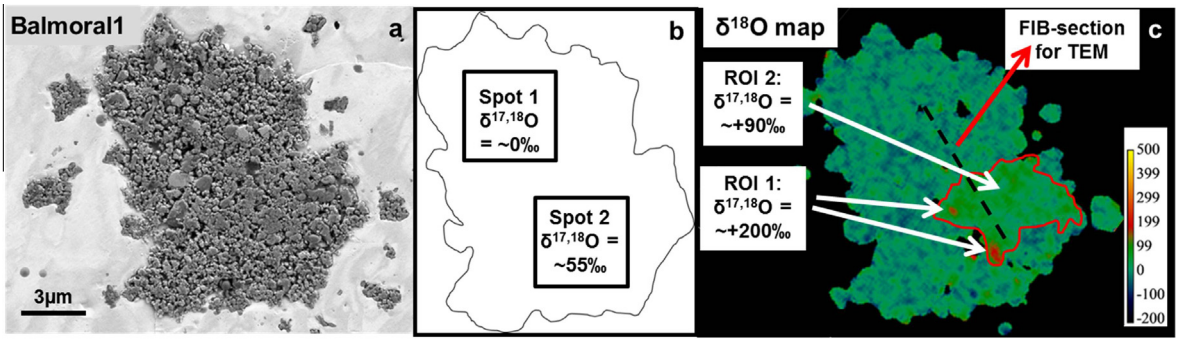

Fig. 2. (a) Secondary electron image of IDP Balmoral1 pressed flat into gold foil showing classic CP-IDP texture. (b) Outline of Balmoral1 showing location of NanoSIMS analytical spots. (c) NanoSIMS isotope map of $\delta^{18}O$ (image processed in Limage software) showing location of $\delta^{18}O$ hotspot region and location where FIB-lift-out was performed (see Fig. 6).

fragment. H, C and N isotope ratios were obtained from NanoSIMS imaging analysis of the bulk fragment and ROIs were drawn in the Limage software to correspond with the O isotope regions as well as areas with distinctive O-isotopic compositions or elemental ratios.

Bulk H, C, and N isotope values for Lumley1 and 2, and Balmoral1, along with Raman spectroscopy data, are reported in Starkey et al. (2013). Isotopic values for the individual regions are presented and discussed here for the first time and are compared to O isotope values determined for these particles.

It is not straightforward to define individual IDPs as either cometary or asteroidal in origin based only on particle texture and/or C/H ratio. Starkey et al. (2013) used Raman spectroscopy to show that Lumley and Balmoral contain organic material that is primitive, particularly in relation to bulk meteorites. In addition, the fine-grained texture and relatively high C/H ratio of Balmoral1 suggests it is anhydrous and CP-IDP-like in nature. CP-IDPs are generally considered to originate from comets. Lumley is more variable but the Raman spectroscopy features (Starkey et al., 2013) suggest that it also originates from either a cometary or primitive asteroidal source that has preserved unprocessed Solar System components.

3.2. Oxygen isotopes: Lumley

The O isotope ratios across the single fragment of Lumley1 vary from $\delta^{17}O$, $\delta^{18}O = -24.3$ (±6.0), −30.8 (±2.5)‰ to 13.7 (±7.8), 19.2 (±5.9)‰, with nearly all analyses falling within error of the Carbonaceous Chondrite Anhydrous Mineral (CCAM) mixing line (Clayton and Mayeda, 1999) and Young and Russell slope = 1 line (Young and Russell, 1998) (Fig. 3). The Lumley1 analyses are compared in Fig. 3 to anhydrous and hydrated IDP data available from previous studies (Aleon et al., 2009; Starkey and Franchi, 2013) that were analysed at a similar level of precision. The O isotope values from different regions of

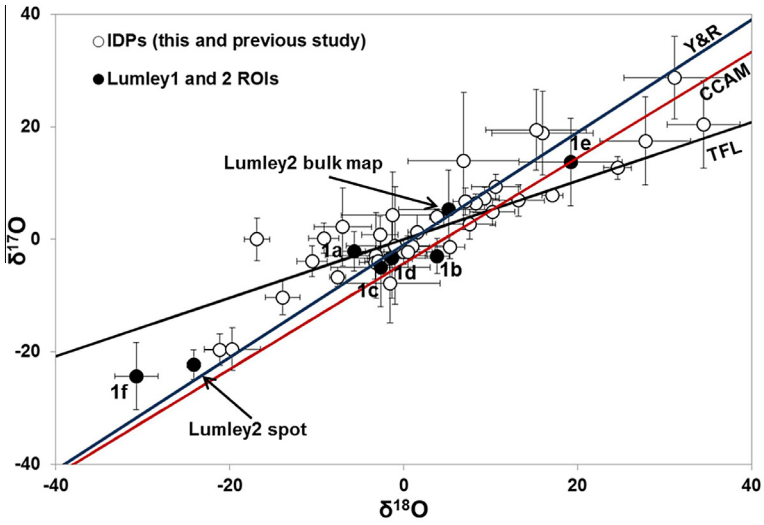

Fig. 3. 3-Oxygen isotope diagram for Lumley1 and Lumley2 spots and images (data in Table 1 and analytical locations on fragment are shown on Fig. 1) in relation to previous measurements of IDPs (Aleon et al., 2009; Starkey and Franchi, 2013). Error bars are shown as 2σ. TFL = Terrestrial fractionation line. Y&R = Young and Russell line (Young and Russell, 1998). CCAM = Carbonaceous chondrite anhydrous minerals line (Clayton and Mayeda, 1999).

Lumley1 cover the entire range of O isotope ratios displayed by IDPs measured in these previous studies.

The isotopic variations in Lumley1 do not, at first, seem to vary systematically across the fragment, with ^{16}O-enriched and depleted areas immediately adjacent to areas possessing what would be considered 'normal' chondritic O isotope ratios ($\delta^{18}O$ = around 0‰) over distances of only a few micrometres. It would appear that the chondritic values occur in areas of the particle that have, on the whole, a fine- to medium- grained texture, but these areas can also contain smoother looking material (i.e., see area 1c Fig. 1) so it is hard to characterise even individual areas of Lumley1 as CP- or CS- like. The ^{16}O-enriched region (area 1f in Fig. 1), with $\delta^{18}O = -30.8$, is the most ^{16}O-enriched signature yet recorded in an IDP. However, area 1f is centred on what appears to be a 'blocky' shaped crystal as opposed to the more typical fine-grained material comprising the rest of the fragment (see Electronic Annex Figure D which is a post-NanoSIMS sputter image revealing that the blocky particle remains even after significant NanoSIMS sputtering so it must have been relatively thick to start with). Therefore, this region should not be considered alongside the other Lumley regions in discussion about the outer solar nebula reservoirs, although it is still interesting in its own right and will be discussed further separately. The heavier O isotope region in 1e (Fig. 1) coincides with a very smooth and featureless region of the fragment which is similar to the texture in some parts of 1b (Fig. 1), that is similarly depleted in ^{16}O. The texture of 1b is a mix of smooth-featureless material and some fine-grained silicates, as indicated by large abundances of Mg and Si in the EDX spectrum of this region.

Lumley2, although smaller, also displays O isotope variability across the particle with the O isotope spot analysis, centred in the area of the particle that is composed of a mixture of extremely fine-grained and possibly smooth/featureless-looking material, giving $\delta^{17}O$, $\delta^{18}O = -22.3$ (±2.6), −24.2 (±0.8)‰ but with the bulk particle O isotope map giving $\delta^{17}O$, $\delta^{18}O = 5.3$ (±7.0), 5.2 (±5.7)‰ (Fig. 3). While these results are very different to each other, a ROI corresponding to the area of the spot analyses gives $\delta^{17}O$, $\delta^{18}O = -16.0$ (±11.0), −23.7 (±7.0)‰, which is within error of the ratio obtained from the spot analysis, and verifies that spot and image analyses can be reliably compared on the same particle. These results show that Lumley2 contains a small region that has a $\delta^{18}O$ around −24‰ with the surrounding region being characterised by more chondritic-like values of $\delta^{18}O \approx 0$‰.

The O isotope signatures in Lumley1 and Lumley2 are variable across each fragment, but covering a similar range. Both fragments contain material with a chondritic O isotope composition which is generally associated with regions that exhibit a fine- to medium- grained texture. Both fragments also contain an ^{16}O-enriched region, although the texture associated with this signature differs between the fragments. In Lumley1 the ^{16}O-enriched region appears to be dominated by a single crystal grain while in Lumley2 the region comprises very fine-grained material. It is only Lumley1 that contains a ^{16}O-depleted region and this is associated with smooth/featureless-looking material. This region has a C/H > 1 so may be composed of anhydrous material.

3.3. Oxygen isotopes: Balmoral1

Two spot analyses positioned at either end of the Balmoral1 particle (~ 10 μm apart) gave O isotope ratios of $\delta^{17}O$, $\delta^{18}O = 1.3$ (±3.1), 1.6 (±1.1)‰ for spot 1 and $\delta^{17}O$, $\delta^{18}O = 56.0$ (±3.0), 55.3 (±1.0)‰ for spot 2 (Figs. 2b and 4). An O isotope ratio map obtained prior

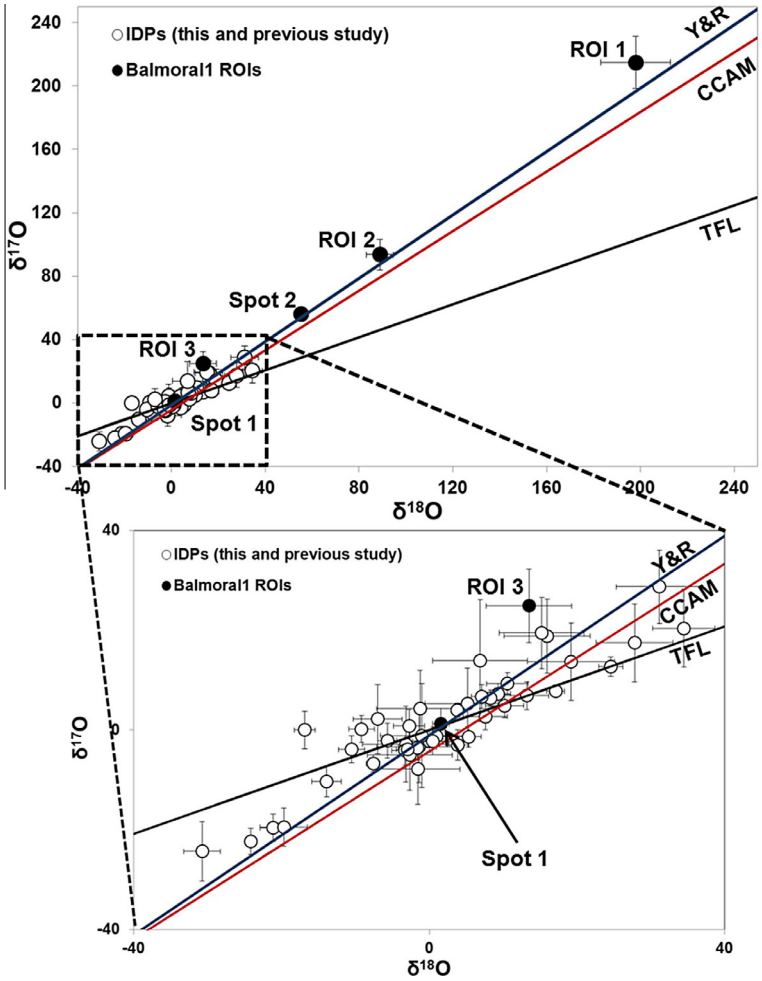

Fig. 4. 3-Oxygen isotope diagram for Balmoral1 spots and images (data in Table 1 and analytical locations on fragment are shown on Fig. 2) in relation to previous measurements of IDPs (Aleon et al., 2009; Starkey and Franchi, 2013). Error bars are shown as 2σ. TFL = Terrestrial fractionation line. Y&R = Young and Russell line (Young and Russell, 1998). CCAM = Carbonaceous chondrite anhydrous minerals line (Clayton and Mayeda, 1999). Lower part of diagram shows zoom in on 'chondrite' region and location of Spot1 that represents the bulk particle composition.

to the spot analyses revealed a bulk particle value of $\delta^{17}O$, $\delta^{18}O = 44.3$ (±5.3), 37.7 (±4.7)‰ (Figs. 2c, 4 and Electronic Annex Figure E). Close inspection of the O isotope ratio image map reveals that one region of Balmoral1 exhibits a much more ^{16}O-depleted ratio, in rough agreement with the spot analysis performed in the same area of the particle. This ^{16}O-depleted region is composed of two small regions (0.5 and 1 μm in size), approximately 3 μm apart, with $\delta^{17}O$, $\delta^{18}O = 215$ (±16), 198 (±14)‰, placing them within error of the slope 1 line (Figs. 2 and 4). These small ^{16}O-depleted regions are surrounded by an area of approximately ~7 μm in size exhibiting smaller, but still significant ^{17}O-, ^{18}O-enrichments, with $\delta^{17}O$, $\delta^{18}O = 93.6$ (±9.6), 88.8 (±5.8)‰, also sitting within error of the slope 1 line. Subtraction of these ^{16}O-depleted regions from the bulk image analysis gives $\delta^{17}O$, $\delta^{18}O = 24.9$ (±7.4), 13.5 (±5.8)‰. An ROI obtained from the O isotope map matched as closely as possible for the area measured as spot 1 gives $\delta^{17}O$, $\delta^{18}O = 21.0$ (±11.5), 11.0 (±7.0)‰. These values should be approximately comparable to spot 1, which falls outside of the ^{16}O-depleted region, but they are instead more ^{16}O depleted, albeit with large uncertainty because of the count-limited precision of the relatively small area. The reason for this discrepancy is not clear. Spot and image O isotope analyses performed on the same regions in other samples (including in Lumley2 and Balmoral1 spot 2) and standards show that the two types of analysis produce comparable results. This, in turn, suggests that the QSA corrections, necessary because ^{16}O is measured on an EM detector for image analyses, are working adequately when the data are processed with the Limage software. QSA corrections are not necessary for the spot analysis because a FC detector is used to measure the ^{16}O isotope in that case. There is no drift observed in the count rates or O isotope ratios during the O spot analysis of Balmoral, suggesting that the sputtered area was stable and that the sample was not sputtered away during the run, which may have otherwise affected the ratio. A remaining option is that, because NanoSIMS analysis is a destructive process, the spot and image analyses produced differing results because

they measured different layers of the sample which may have differed with depth. The image analysis clearly seems to have analysed material that is more ^{16}O-depleted, which may be due to the presence of fine-grained ^{16}O-depleted material within the region of spot 1, that was preferentially sputtered away during the image analysis prior to performing the spot analysis.

In order to help clarify the discussion, the very ^{16}O-depleted region ($\delta^{18}O = 198‰$) composed of two very small areas, will be termed ROI 1. The intermediate O isotope region ($\delta^{18}O = 88.8‰$) surrounding the very ^{16}O-depleted material will be termed ROI 2. The rest of the fragment (bulk fragment minus ROI 1 and 2) will be termed ROI 3.

SEM imaging reveals a subtle difference in the particle texture between ROI 1, 2 and ROI 3 (Fig. 2 and Electronic Annex Figure C). All ROIs are ultra-fine-grained but ROI 1 and 2 appear to be more compact, and the isotopic variability within ROI 2 is much less than that displayed by ROI 3, with a relatively sharp boundary between these regions (Fig. 2c). In addition, the isotope map shows the presence of fine-grained, ^{16}O-depleted material, possibly related to ROI 2, unevenly dispersed throughout parts of ROI 3 (Fig. 2 and Electronic Annex Figure E).

3.4. H, C, N, O isotopic variability: Lumley

The data presented here for Lumley1 are from the same set of analyses as those presented for these fragments in Starkey et al. (2013) but the data have been further processed to reveal the isotopic composition of H, C and N associated with the same areas that were analysed for O isotopes. A different area of the Lumley 2 fragment was analysed for H, C and N isotopic composition to that analysed for O and so these data are not compared.

The Lumley 1 data make it possible to compare different isotope systems across a single IDP fragment to assess micrometre-scale intra-fragment isotopic variability of silicate ($\delta^{18}O$) and organic (δD, $\delta^{13}C$ and $\delta^{15}N$) components. δD, $\delta^{13}C$ and $\delta^{15}N$ values for the six individual areas of Lumley 1 are presented in Table 1 along with the C/H ratios. The data are also shown in Fig. 5 where the values are plotted against $\delta^{18}O$ because Lumley1 shows large O isotope variability and $\delta^{18}O$ indicates the relative placement of the analysis along the CCAM line. $\delta^{18}O$ is matched to δD, $\delta^{13}C$ and $\delta^{15}N$ for each individual region measured in Lumley1 (areas shown in Fig. 1 and Limage δD, $\delta^{13}C$, $\delta^{15}N$ and C/H images in Electronic Annex Figure G). The intra-fragment co-variation between the various isotope systems appears to show broadly positive relationships of δD, $\delta^{13}C$ and $\delta^{15}N$ with $\delta^{18}O$, although none of the correlation coefficients are significant at more than the 90% level.

3.5. H, C, N, O isotopic variability: Balmoral1

Bulk H, C, and N isotope compositions for the Balmoral1 fragment are reported in Starkey et al. (2013) but the raw data have been reprocessed here in the same way as for the Lumley1 results in order to observe the finer-scale detail. Maps of δD, $\delta^{13}C$, $\delta^{15}N$ and C/H for Balmoral1 are available in Electronic Annex Figure H. Despite the small volumes of material being investigated, it was possible to generate δD, $\delta^{13}C$ and $\delta^{15}N$ values for ROI 2 and 3 along with the element ratios C/H, Mg/Si, Mg/O and Si/O from the NanoSIMS mapping (see Table 1 and Electronic Annex Table A). It was not possible to obtain all the ratios for ROI 1 (e.g., $\delta^{13}C$, $\delta^{15}N$ and C/O) because the ^{16}O-depleted region could not be accurately matched up onto the NanoSIMS images that were performed without O isotope ratio measurements.

The silicate element ratios reveal that ROI 2 does not have a composition lying between that of ROI 1 and 3, as might have been expected from its intermediate O isotope composition. ROI 1 and 2 have C/H = ~0.6 indicating that these areas of the IDP are hydrated whereas ROI 3 has C/H = ~1.2 suggesting it is more anhydrous in nature. ROI 3 gives a bulk $\delta D = 1000$ (±34)‰ whereas the more ^{16}O-depleted ROIs 1 and 2 give $\delta D = 493$ (±182)‰ and 502 (±56)‰, respectively, indicating that they are characterised by a depletion in D compared to the bulk fragment. C and N isotopes are not available for ROI 1 but ROI 2 and 3 give very similar values with $\delta^{13}C = -44$ (±8) and $\delta^{15}N = 248$ (±17) for ROI 2 and $\delta^{13}C = -42$ (±2)‰ and $\delta^{15}N = 272$ (±5)‰ for ROI 3.

3.6. TEM investigation of mineralogy of ^{16}O-depleted region

STEM-EDX and HR-TEM imaging was performed on a FIB lift-out which cuts across the Balmoral1 fragment to obtain a section of ROI 2 and ROI 3 (see Figs. 2 and 6 and Electronic Annex Figure I). Unfortunately, because of their very small spatial extent, the very ^{16}O-depleted regions (ROI 1; $\delta^{18}O = 198‰$) were missed on sectioning.

TEM images reveal Balmoral1 is composed of an aggregate of small grains which are, on the whole, in the 20–80 nm range, held within areas of finer-grained and/or a small amount of amorphous material (Fig. 6). Those minerals large enough to be identified include clinopyroxene, orthopyroxene and olivine, which has a composition towards the forsteritic endmember. Ni-bearing Fe-sulphides (pyrrhotite and pentlandite) and magnetite are also present in smaller quantities. Where possible (i.e., where the FIB section was thin enough and the individual minerals were not overlapping), lattice fringe imaging to obtain mineral d spacings was performed from HRTEM images and revealed the likely presence of clinoenstatite (spacing of (1 0 0) planes = 0.91 nm), pentlandite (spacing of (2 0 0) planes = 0.5 nm) and either pentlandite or olivine (spacing of (3 1 1) planes = 0.3 nm), in keeping with the results from STEM-EDX (Fig. 6).

Fig. 6 (and Electronic Annex Figure IH) shows how the FIB lift-out section corresponds with the original ion images and, therefore, how the mineralogy relates to the isotopic signatures across Balmoral1. Clinopyroxene, orthopyroxene and olivine constitute a large part of the section, from ROI 3 into the more ^{16}O-depleted ROI 2. A relatively large olivine grain can be seen in Fig. 6d which is in ROI 3 of Balmoral1. These mineral phases are consistent with those expected in IDPs, along with C-rich phases (Mackinnon and Rietmeijer, 1987) which may be

Table 1
Oxygen, carbon, nitrogen and hydrogen isotope data along with C/H and uncalibrated ion ratios for C^-/O^- and CN^-/O^- for Balmoral1, Lumley1 and Lumley2.

Name	Texture	Analysis type O	$\delta^{17}O$	$\delta^{17}O$ error	$\delta^{18}O$	$\delta^{18}O$ error	$D^{17}O$	$D^{17}O$ error	$\delta^{13}C$	$\delta^{13}C$ error	$\delta^{15}N$	$\delta^{15}N$ error	δD_{SMOW}	δD_{SMOW} error	$^{12}C/^{1}H$	Area H, C, N (μm)	C^-/O^-	C^-/O^- error
Lumley 1a	FG blocky	Spot	−2.1	3.5	−5.7	1.3	0.8	2.5	−22	16	334	27	702	223	1.3	25	0.00088	3.75E-05
Lumley 1b	Smooth/ Textureless	Spot	−3.0	3.1	3.9	1.4	−5.0	2.8	17	16	498	31	480	127	1.1	25	0.00095	4.31E-05
Lumley1c	FG blocky	Image	−5.0	7.0	−2.7	5.7	−3.6	9.1	−14	11	259	15	531	122	1.1	64	0.00038	1.17E-05
Lumley1d	FG blocky	Image	−3.4	7.1	−1.4	5.8	−2.7	9.1	−25	10	316	15	575	119	0.8	49	0.00051	1.53E-05
Lumley1e	Smooth/ Textureless	Image	13.7	7.8	19.2	5.9	3.7	9.8	−4	16	553	35	861	153	1.1	64	0.00065	3.00E-05
Lumley1f	Compact/ blocky	Spot	−24.3	6.0	−30.8	2.5	−8.3	5.6	−46	28	236	30	495	245	0.5	25	0.00017	1.37E-05
Lumley2 spot	FG compact	Spot	−22.3	2.6	−24.2	0.8	−9.7	1.7	No map exists for same area									
Lumley2 bulk	Mixed	Image	5.3	7.0	5.2	5.7	2.6	9.1	No map exists for same area									
Balmoral1 Spot 1	FG porous	Spot	1.3	3.1	1.6	1.1	0.4	1.8	−33	13	351	28	1128	128	0.8	25	0.000213	9.44E-06
Balmoral1 Spot 2	Mixed FG	Spot	56.0	3.0	55.3	1.0	27.2	1.6	−26	10	178	22	498	100	0.9	25	0.000358	1.27E-05
Balmoral1 ROI 1	FG compact	Image	215.0	16.4	198.0	14.9	112.0	22.1	No map exists for same area				493	182	0.6			
Balmoral1 ROI 2	Mixed FG	Image	93.6	9.6	88.8	5.8	47.4	11.2	−44	16	248	34	502	112	0.6	25	0.000151	7.34E-06
Balmoral1 ROI 3	Mixed FG	Image	24.90	7.4	13.5	5.8	17.8	9.5	−42	2	272	5	1000	34	1.2	140	0.000350	4.47E-06

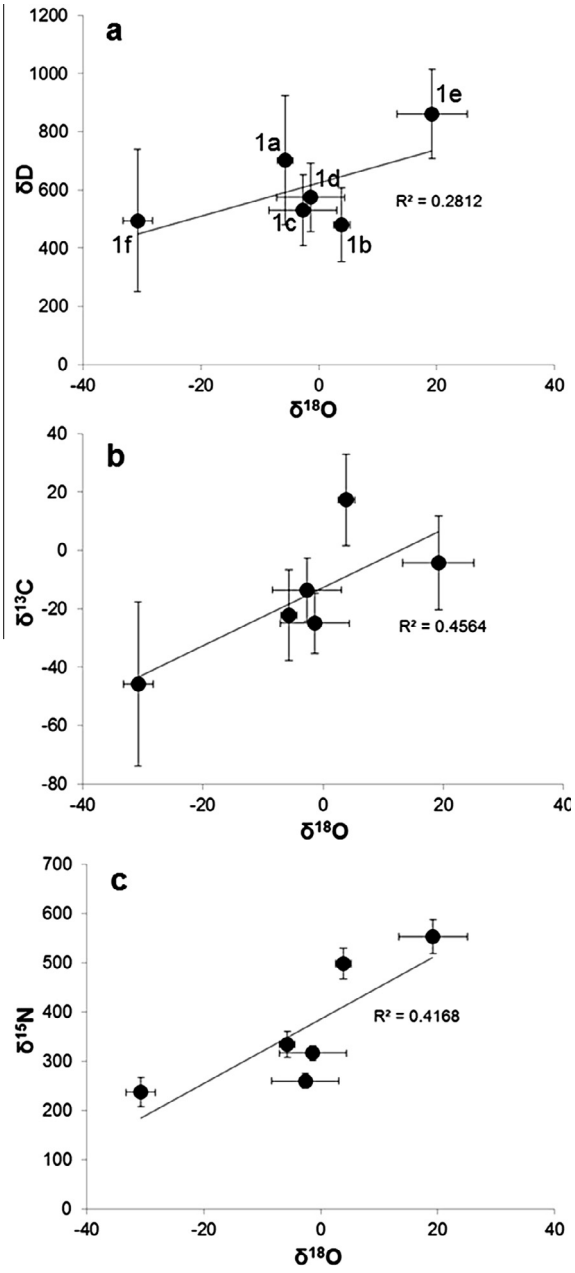

Fig. 5. Correlated $\delta^{18}O$ versus (a) δD, (b) $\delta^{13}C$ and (c) $\delta^{15}N$ for individual regions of Lumley1 (data in Table 1 and analytical locations on fragment are shown on Fig. 1). Error bars are shown as 2σ.

represented by the small amount of amorphous material seen in Balmoral1. Although a lot of fine-grained material in an amorphous matrix was observed in the TEM section, the composition of the small grains was not identified and so it is not possible to confirm whether this material is GEMS. However, the exact texture does not appear to resemble GEMS that has been observed in other TEM studies of IDPs. Pyrrhotite and magnetite are observed in ROI 3 but it is only pentlandite that is observed along with the olivine and pyroxenes in ROI 2 (Fig. 6). Pentlandite is often cited as indicating that an IDP is hydrated, which would be in keeping with the lower C/H ratio determined for ROI 1 and 2 and their more compact appearance, and lack of isotopic variability in ROI 2. The FIB-lift-out only covers a very small region of Balmoral1 and most of the minerals are too fine-grained (tens of nanometres in size or less) to identify definitively, even by TEM. Therefore, there may be additional mineral phases present to those observed by TEM. The presence of magnetite in Balmoral1, albeit in small quantities, may indicate that the IDP experienced heating during atmospheric entry. However, Fraundorf (1981) stated that the presence of fine-grained magnetite within IDPs may not necessarily be a result of atmospheric heating but instead represent a primary phase. Importantly, in Balmoral1, no observation was made of magnetite as rims on sulphides, which would have otherwise supported the idea of atmospheric heating. In addition to this, the isotopic variation observed is not falling on a mixing line to terrestrial oxygen (with $\delta^{18}O \sim +50‰$; as shown by micrometeorites) which indicates again that there was no significant terrestrial O contribution that could have occurred during heating. As such, the evidence suggests that Balmoral1, particularly the isotopically anomalous region, did not experience significant atmospheric heating.

4. DISCUSSION

4.1. Micrometre-scale isotopic diversity in the comet-forming region: Implications from IDP Lumley

Such wide O isotope variability as that seen at the micrometre-scale in Lumley has not been observed in a single IDP fragment previously. The isotopic variability measured in Lumley provides some important clues about the formation history of the Lumley parent body, whether it was a primitive asteroid or a comet, and about the silicate and organic reservoirs of the early Solar System. The Raman D and G band parameters of the organic matter in Lumley indicate that this material is more primitive than insoluble organic matter (IOM) extracted from bulk meteorites (see Starkey et al., 2013). Assuming that there is a common organic reservoir of organic matter in the early solar nebula, as argued for by Alexander et al. (2007), Alexander et al., 2012, this indicates that at least some portion of the Lumley parent body experienced very little, or no, processing compared to that experienced by carbonaceous chondrites.

To account for the variable isotopic, elemental and textural features across Lumley1 it is possible that the Lumley parent body formed from varying mixtures of at least three discrete reservoirs. Reservoir 1, represented by Lumley 1f, is relatively pristine, retaining a more solar-like, ^{16}O-enriched signature with relatively low δD, $\delta^{13}C$ and $\delta^{15}N$. The C/H for Lumley 1f is low but the measured C/O ratio is also low compared to other areas of Lumley, indicating a low C abundance as opposed to it being hydrated. The texture of Lumley 1f is blocky/compact, which together with the isotopic and elemental compositional information available, suggests that it is a refractory grain originating from the inner Solar System, such as a CAI. A grain presumed

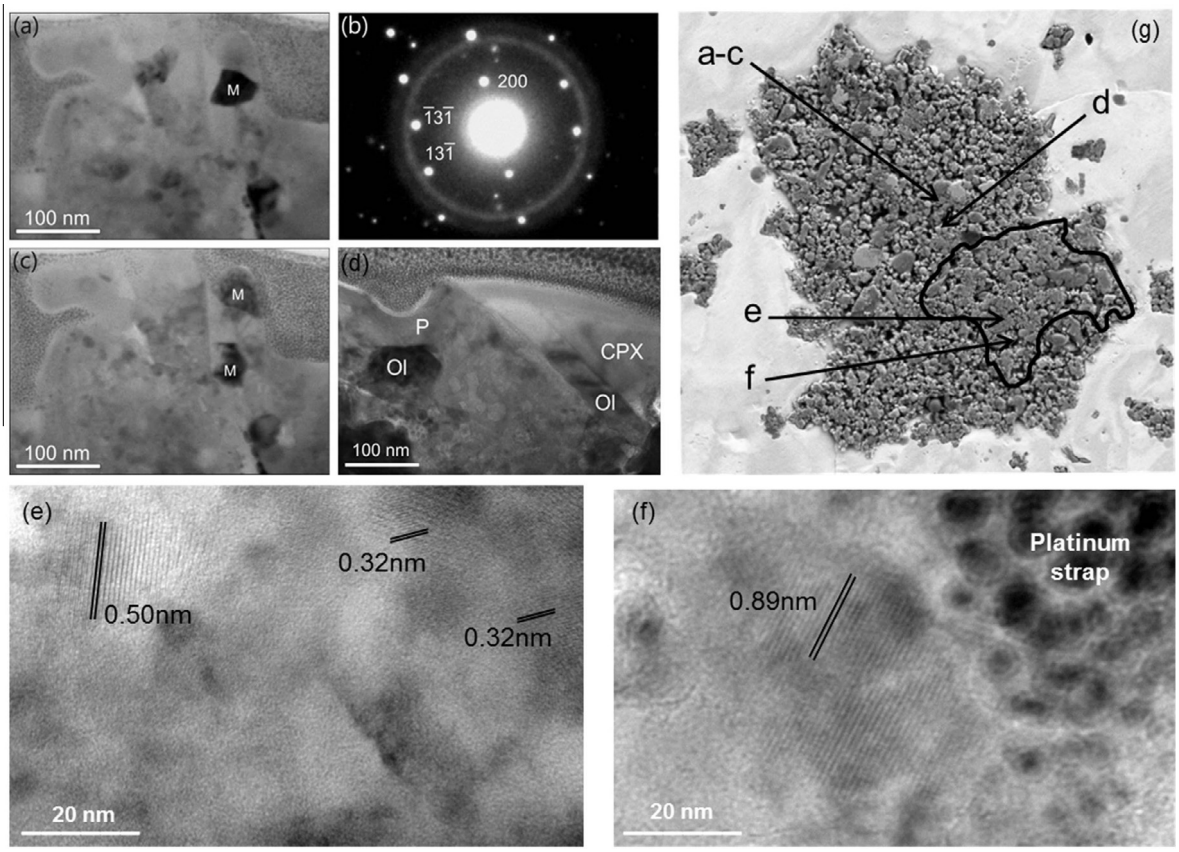

Fig. 6. (a) Bright-field TEM images and (b) a SAED pattern of magnetite (M) in an area of Balmoral1 (see (g) and Electronic Annex for location). The SAED pattern in (b) was acquired from the magnetite crystal in (a) and shows the [0 1 3] zone axis. The superimposed rings are from the FIB-deposited platinum, and the innermost ring is {1 1 1} with a d-spacing of 0.2265 nm. (c) Bright-field TEM images of magnetite (M) of same area as (a) but acquired at different degree of tilt of the goniometer specimen holder. Four magnetite crystals are present, and the degree to which they scatter electrons varies with their orientation relative to the electron beam (i.e., where black they are satisfying Bragg condition). (d) Bright-field TEM image of an area of Balmoral1 (see (g) and Electronic Annex for location) containing crystals of olivine (Ol), clinopyroxene (Cpx) and pyrrhotite (P). The olivine crystal is being viewed parallel to [0 0 1] and the terminations on its right hand side are parallel to the traces of (0 1 0) and (1 1 0) planes. The finely granular material along the top edge of the image is the base of the platinum strap, and the black areas in the lower left and lower right are the Al substrate. (e) Lattice d spacings in an area of Balmoral1 located within the ^{16}O-depleted region (see (g) and Electronic Annex for location) showing spacings corresponding to pentlandite (spacing = 0.5 nm and 0.3 nm) and f) for clinoenstatite (0.9 nm) where the solid lines are shown perpendicular to the spacings and the value of the spacing is shown adjacent.

to be a CAI was observed as a terminal particle collected by Stardust from comet 81P/Wild2 (Inti; Simon et al., 2008) and provides evidence for outward radial transport of inner Solar System solids to the comet-forming region (Zolensky et al., 2006; Nakamura et al., 2008; Bridges et al., 2012; Ogliore et al., 2012). The presence of CAIs in comets was actually a prediction of the bipolar outflow X-wind model of Shang et al. (2000), but radial transport of material outwards by turbulent flow is also a plausible mechanism to move inner Solar System materials to large AU (Bockelée-Morvan et al., 2002; Ciesla, 2007).

Reservoir 2, represented by Lumley 1a, 1c and 1d that exhibit a fine-grained CP-IDP-like texture, has chondritic-like $\delta^{18}O$ (~0‰), relatively low δD, $\delta^{13}C$ and $\delta^{15}N$ but variable C/H. The isotopic signatures of the material forming these regions are similar to that of many carbonaceous chondrites. It would appear that Reservoir 2 is dominated by fine-grained dust from the same chondritic reservoir as was sampled by most asteroids, most likely originating in the inner parts of the protostellar disk, that was subsequently transported out to the comet-forming region at larger AU by radial transport (e.g., McKeegan et al., 2006; Nakamura et al., 2008). The variable C/H ratios across these regions may indicate that there is a mix of anhydrous and hydrated material but this parameter does not co-vary with $\delta^{18}O$. However, low C/O ratios for 1c and d (see Table 1) indicate that these regions have a low C abundance and therefore are still largely anhydrous in nature.

Reservoir 3 is represented by Lumley 1b and 1e that exhibit a smooth/amorphous texture and high C/H and C/O ratios. $\delta^{18}O$ values for Lumley 1b and e are relatively high (= +3.9‰ (1b), 19.2‰ (1e)), with variable δD (= 480‰ (1b), 861‰ (1e)) and high $\delta^{13}C$ (= 17‰ (1b) and −2‰ (1e) and $\delta^{15}N$ (= 498‰ (1b) and 553‰ (1e)). NanoSIMS ion images (available in Electronic Annex Figure G) illustrate these features, with brighter pixels showing high

$\delta^{15}N$ in the 1b and 1e regions. Although the δD of 1b is not as high as 1e, the NanoSIMS D/H ion image (Electronic Annex Figure G) shows that the majority of the material comprising 1e has a δD value closer to that of 1b, and that the high δD for 1e may be dominated by a small region (around 2 μm in size) with high δD within the area defined as 1e. The high $\delta^{18}O$ values are comparable to the O isotope signatures for hydrated IDPs, that tend to fall above $\delta^{18}O = 0‰$ (e.g., Aleon et al., 2009; Starkey and Franchi, 2013). Although the higher C/H ratios suggest that the silicates may be predominantly anhydrous, these values coupled with high C/O could instead suggest a high abundance of C. However, the high δD and $\delta^{15}N$ signatures in these Lumley regions, coupled with the presence of $\delta^{15}N$ hotspots up to several thousand permil (Electronic Annex Figure J), indicate this material is primitive. As such, it is unlikely this material has experienced processing within the inner protostellar disk or on a parent body, as such signatures are thought to be destroyed during processing, particularly those of the presolar grains (Nguyen and Zinner, 2004). The elevated organic isotope signatures also indicate a cometary source as these are high where they have been determined for comets (Robert, 2006 and references therein; Arpigny et al., 2003; Bockelée-Morvan et al., 2008; Mumma and Charnley, 2012). The evidence, therefore, suggests an origin in the outer Solar System for these Lumley regions.

The isotopic and textural variation between discrete areas, in Lumley1, that are separated by only a few micrometres, have distinct formation histories before ultimately being assembled on the Lumley parent body. The material in each of these areas draws upon components from different reservoirs with distinct isotopic signatures that were affected by, as yet undefined, processes to produce different textures. The detail apparent in the NanoSIMS ion images (Electronic Annex F) reveals that the bulk values for the regions defined here in Lumley1 may not be restricted to sampling only one particular lithology (or reservoir) and may themselves encompass a mix of material.

The limited data for IDPs measured for O isotopes previously (Aleon et al., 2009; Starkey and Franchi, 2013) have shown a relatively homogenous composition (except for presolar grains) within single particles indicating that individual IDPs sample a well-mixed local reservoir. Starkey and Franchi (2013) suggested from a study of a collection of fine-grained IDPs that the more chondritic (less ^{16}O-rich) IDPs originated from parent bodies that formed at smaller heliocentric distance where the mix of inner Solar System versus outer solar nebula dust was much higher. Conversely, the more ^{16}O-rich IDPs originated from parent bodies formed at larger heliocentric distance where the influx of inner Solar System dust to the mix was lower. Size-density sorting of silicate and sulphide grains observed in CP-IDPs and Wild2 provide further evidence of transport mechanisms in the comet-forming region that may also be a function of heliocentric distance (Wozniakiewicz et al., 2012). In addition, CP-IDPs that have the smallest grain sizes are also reported to contain the highest abundances of amorphous silicates and circumstellar grains (Bradley, 2003; Nguyen et al., 2007; Wirick et al., 2009).

Lumley, a single fragment from a cluster IDP, appears to sample a range of reservoirs and/or lithologies. This implies that the Lumley parent body sampled mixtures from a range of AU. These materials, represented by different lithologies and isotopic signatures, appear to have been incorporated into the Lumley parent body as individual clasts at the several micrometre-scale, themselves composed of nanometre-sized grains, rather than as individual grains of fine-grained dust. These clasts, although they do not display sharp boundaries, are apparent from the diverse textures and isotopic signatures observed. The formation of each clast, presumably originally from the aggregation of fine-grained dust, must have occurred at an earlier time, possibly in a different location, followed by disruption of these materials before final re-aggregation on the Lumley parent body. It is not clear if these micrometre-scale fragments represent aggregates that were formed in the protostellar disk, of a series of larger bodies that were subsequently disrupted and dispersed.

Alternatively, the distinct areas in Lumley may all originate from a single parent body that incorporated material from only one reservoir which was subsequently altered in situ on the parent body. Although details of the original inter-relationship of the areas has been lost when the particles were pressed in gold, the intimate mix of very different reservoirs is difficult to reconcile with any scenario involving modification in situ at such a fine-scale; altering some regions and not others to produce the diverse range of compositions observed. Complex mixes of material are frequently observed in primitive meteorites (e.g., Burbine et al., 2002; Bischoff et al., 2006 and references therein; Abreu, 2013), but in this case the aggregated clasts are at least an order of magnitude larger. Such mixes are generally believed to have formed by brecciation processes on asteroidal bodies.

The ^{16}O-rich grain (reservoir 1) in Lumley 1f appears to be a fragment of a refractory grain, providing evidence of material from the innermost regions of protostellar disk being delivered to the Lumley parent body formation zone, most probably by turbulent mixing processes (Bockelée-Morvan et al., 2002; Ciesla, 2007). The size of this grain fragment is approaching that of the other regions in Lumley, which may indicate that it was incorporated as a discrete fragment at the time of Lumley final accretion. This may indicate that transport of inner disk material was still being delivered to the Lumley at the time of final accretion.

4.2. Origin of O isotopic heterogeneity in Balmoral1

The O isotope ratios measured in ROI 1 and 2 of Balmoral1 are considerably more enriched in ^{17}O and ^{18}O than any ratios measured in IDPs to date (e.g., Aleon et al., 2009; Starkey and Franchi, 2013), other than those found in rare sub-micrometre pre-solar grains. These ratios are also much more ^{16}O-depleted than O isotope ratios obtained for bulk meteorites. ROI 1 is composed of two discrete areas with essentially identical ^{17}O, ^{18}O enrichments. There are no large, discrete grains coinciding with the location of the ROI 1 hot spots and therefore these areas must be composed of aggregates of small grains.

There is clearly a strong relationship between the material in ROI 1 and ROI 2, discussed below, such that this feature needs to be considered as a distinct entity. The size of ROI 1 and ROI 2, and the large number of grains associated with this enrichment, is unlike any previously identified pre-solar grain. The texture apparent in the SEM images appears typical of fine-grained CP-IDPs and so it would appear extremely unlikely that this material has a pre-solar circumstellar origin. Although the composition of ROI 1 and 2 overlaps with that of some possible presolar grains reported in the literature (Nguyen et al., 2010; Keller and Messenger, 2011), the relatively large size of the enriched region in Balmoral1 sets it apart from these grains. In addition, ROI 2 appears to be roughly chondritic in composition and is composed of a multi-grain clast that looks similar to normal IDP material. It would seem unlikely that such a complex mix of phases could be generated and aggregated together from a single nucleosynthetic event so it is suggested that this material is not presolar in origin.

Almost all early solar nebula components (CAIs, chondrules, mineral fragments) found within meteorites have oxygen isotopic compositions that fall along a mixing line with a slope of approximately 1. Their isotopic compositions range from around the solar value ($\delta^{17}O$, $\delta^{18}O = -59.1‰$, $-58.5‰$), as determined from the Genesis solar wind samples (McKeegan et al., 2011), up to values around $+10‰$ in $\delta^{17}O$, $\delta^{18}O$ (Clayton, 1993). The origin of this variation remains elusive, although isotope selective self-shielding (Clayton, 2002) is one of the most plausible mechanisms to account for the non-mass dependent variations in O isotope compositions observed in the Solar System. However, this mechanism requires a reservoir enriched in the heavy isotopes of O. In order to impart the signature of this reservoir into large amounts of solid silicate material it is generally inferred that abundant, and reactive, water was involved. Identification of a ^{16}O-depleted primordial water reservoir in the early Solar System, and its distribution and interaction with the rock record, is currently not well established.

O isotope compositions similar to those in ROI 1 in Balmoral1 have been found in one other instance, in the meteorite Acfer 094, where $\delta^{17}O$, $\delta^{18}O$ values around $+200‰$ were reported (Sakamoto et al., 2007). Although, as noted above, both Nguyen et al. (2010) and Keller and Messenger (2011) report presolar grains with compositions in error of CoS. The presence of large ^{16}O depletions in Acfer 094 was presented as evidence for interaction of the Acfer 094 parent body, or components within it, with primordial water strongly depleted in ^{16}O (Sakamoto et al., 2007; Seto et al., 2008). The material containing the ^{16}O-depleted signature was originally termed new-PCP (poorly-characterised phase) by Sakamoto et al. (2007) but was later named cosmic symplectite (CoS) after further investigation by Seto et al. (2008). CoS is distributed ubiquitously in the matrix of Acfer 094 and TEM results reveal its 'wormy'-like symplectite texture, composed of intergrown magnetite and pentlandite (Seto et al., 2008). One formation mechanism proposed for CoS is that it forms from Fe-metal or Fe-metal sulphide that has been radially transported out from the inner Solar System, sulphurised to Fe sulphide as the ambient temperature drops, and oxidised to magnetite by water vapour moving in from the outer solar nebula (Sakamoto et al., 2007; Seto et al., 2008). Alternatively, it was suggested that CoS may have formed by oxidation on the parent planetesimal, in the very earliest stages of aqueous alteration, prior to the onset of hydrous mineral formation (Sakamoto et al., 2007; Seto et al., 2008). It is possible that a signature of interaction with primordial water could be available in Acfer 094 because of its very primitive, unaltered nature (ungrouped type 3.0) meaning that the signature did not decompose during subsequent alteration (Abe et al., 2011). If this is correct then cometary samples should be expected to contain CoS because of their primitive nature. Indeed, Yurimoto and Kuramoto (2004) suggest that the O isotope composition of cometary ices should lie in the range of $\delta^{18}O = +50‰$ to $+200‰$. However, no evidence of CoS-like material or such ^{16}O-poor material has previously been reported in cometary samples (IDPs and Stardust) prior to this study.

The size of the ^{16}O-depleted regions (ROI 1 and 2) in Balmoral1 are similar in size to the regions containing similar O isotope signatures observed in Acfer 094, which can be as large as 160 μm but with most being less than ten micrometres. The presence of Fe- and Fe-Ni-bearing minerals in Balmoral1 do not, on their own, necessarily confirm the presence of CoS because these minerals are observed commonly in IDPs that do not exhibit extreme ^{16}O-depleted signatures (Zolensky and Thomas, 1995). In addition, the symplectite 'CoS' texture documented in Acfer 094 (Seto et al., 2008) is not observed in the Balmoral1 FIB-section. However, of the ^{16}O depleted regions present in Balmoral1, only ROI 2 was sampled by the FIB section. As only ROI 1 displays ^{16}O depletions comparable to CoS, there is no direct evidence for the nature of the mineralogy of the most extreme ^{16}O depletions in Balmoral1. However, two lines of evidence provide a strong indication that ROI 1 has a mineralogy quite distinct from that of CoS. Firstly, if the isotopic signature of ROI 2 were the result of mechanical mixing of ROI 1 material and "normal" IDP material ($\delta^{17}O$, $\delta^{18}O \approx 0‰$), then ROI 2 should contain approximately 50% of ROI 1 material. That there is not an abundance of pentlandite and magnetite in the FIB-section sampling ROI 2 rules out mechanical mixing of a CoS-like assemblage. Secondly, the measured ratio of ^{16}O- and ^{28}Si-ion intensities for ROI 1 is essentially identical to that of ROI 2 and 3 (Electronic Annex Table A). This is inconsistent with any significant CoS-like material being present as CoS is essentially devoid of Si (Seto et al., 2008) and, therefore, would be expected to generate a large shift in the measured $^{16}O^-/^{28}Si^-$ signal. The FIB-section reveals that ROI 2 and 3 are primarily composed of ferromagnesian silicates and, therefore, it would appear that ROI 1 is also dominated by such phases.

Although ROI 1, 2 and 3 are all primarily composed of ferromagnesian silicates, the $^{24}MgO^-/^{16}O^-$, $^{28}Si^-/^{16}O^-$ and $^{24}MgO^-/^{28}Si^-$ ion ratios of ROI 2 are not intermediate between those of ROI 1 and 3. Therefore, it can be concluded that the intermediate O isotopic composition of ROI 2 is not the result of mechanical mixing of ROI 1

material with that of the surrounding ROI 3. Mixing of ROI 1 with other CP-IDP-like material prior to final accretion on the Balmoral parent body is also considered unlikely as the homogeneous O isotope composition of ROI 2 (see Fig. 2) requires exceptionally efficient mixing of two components, potentially differing by over 200‰. As discussed earlier, it appears likely that ROI 1 and 2 share a common origin but that they then experienced variable, or selective, processing, interacting with an O isotope reservoir quite distinct from the starting composition. The C/H (0.6) of ROI 2 is very low, typical of CS-IDPs, and generally taken as indicative of aqueous alteration (e.g., Aleon et al., 2001). Certainly, the rather homogeneous O isotope composition of ROI 2 is more consistent with that expected from aqueous alteration than would be expected from CP-IDP-like material that contains a wide variety of components (e.g., Keller and Messenger, 2011). The presence of pentlandite within ROI 2 is indicative of some aqueous alteration, and the possible lack of GEMs. ROI 2 is also devoid of any isotopically anomalous D hot spots (see Electronic Annex Figure K). Such characteristics are all consistent with the effects of aqueous alteration of primitive material.

If aqueous alteration played a role in establishing the distinct O isotope composition of ROI 1 and ROI 2, it is unclear whether it was the fluid or the initial silicate material that was heavily depleted in ^{16}O. Small shifts in $\delta^{18}O$ along a slope = ½ line could be affecting the isotopic composition of the altered material within Balmoral. For example, the effect in the carbonaceous chondrites is around 6‰ and so comparable effects could easily be lost in the uncertainty of any slope defined with the ROI 1 composition as an endmember. Indeed, the uncertainties on the larger ROI 2 measurement are comparable to this 6‰ effect. However, these effects are very small compared to the difference in the endmember compositions required in the mixing. It may be that ROI 1 and 2 were both originally heavily depleted in ^{16}O ($\delta^{18}O \approx 200‰$) and that their interaction with more typical Solar System water ($\delta^{18}O \approx 0‰$) at a late stage resulted in some exchange which shifted ROI 2 material towards the water composition, while ROI 1 remained largely, or completely unaffected. Alternatively, ROI 1 and ROI 2 may both have been typical of protostellar disk material ($\delta^{18}O \approx -50‰$ to 0‰) but then interacted with water heavily depleted in ^{16}O. In this scenario ROI 1 would be represented by areas where exchange (or alteration) was complete while ROI 2 represents areas where alteration was only partial. However, there is limited information available on ROI 1, and therefore it is difficult to establish the exact nature of the relationship between ROI 1 and ROI 2.

The δD of ROI 1 and ROI 2 is ≈500‰, considerably more D-depleted than pristine CP-IDP material (e.g., Messenger, 2000, 2002; Starkey and Franchi, 2013). Any aqueous alteration would have had a pronounced impact on the δD and therefore it would appear that the fluid was depleted in D. Given the common δD and C/H of ROI1 and ROI2 it is more likely that both regions are aqueously altered, with ROI 1 being more completely altered and reflecting the composition of the fluid.

The distinct boundary to ROI 1 and 2 indicates that this component was incorporated into the Balmoral IDP ROI 3 material as a distinct clast after the alteration event. However, the formation of ROI 3 itself is not straightforward because it also displays an elevated O isotope signature in relation to chondrites, albeit one much less than that displayed by ROI 1 and 2. Based on information provided by the NanoSIMS O isotope ratio images (Electronic Annex Figure E) it is proposed, despite its higher than chondritic O isotope bulk signature, that ROI 3 is primarily composed of fine-grained typical CP-IDP-like chondritic material with $\delta^{18}O \leqslant 0‰$. However, it must also contain material with a similar O isotope composition to ROI 1 and/or 2 (with unknown but high $\delta^{18}O$ of +90‰ to +200‰). The O isotope ratio images (Electronic Annex Figures H and K) show that there are numerous small fragments (<1 μm in size) of material with isotopic compositions similar to ROI 2, particularly in the lower half of the particle more adjacent to ROI 2. This indicates that during the final accretion event(s) that formed the Balmoral parent body, further disruption of the ROI 1, 2 clast occurred to fragment them and mix this material locally with the more typical CP-IDP material. The high δD signature of ROI 3 reflects the abundant D-rich organic material present in the more abundant CP-IDP component of ROI 3.

These results indicate that there are some broad similarities between Lumley and Balmoral. Both IDP fragments are composed of an aggregate of small (several-micrometre) sized clasts where the clasts can exhibit a wide range in isotopic signatures and lithology. As discussed above, it seems possible that these clasts were originally formed from primary fine-grained dust in different settings (place and/or time) that were characterised by different lithological, elemental and isotopic characteristics (silicate and organic). It is proposed, based on the primitive nature of the IDPs, that these original reservoirs had to be located at relatively large AU. Subsequent disruption of these materials/reservoirs/early bodies, possibly through collisional events, then their re-incorporation as micrometre-sized clasts into new bodies (the parents of the Lumley and Balmoral particles) could account for the observations seen. The small size of the clasts in relation to those observed in brecciated chondrites may be related to the more primitive and fragile (loosely bound) nature of the early Solar System dust that formed these original reservoirs/bodies, a reflection of the limited processing experienced by these bodies. This could be a function of a number of parameters such as limited alteration processes or the small size of the intermediate bodies involved in the assembly, disruption, and final accretion that ultimately led to the formation of comets.

4.3. Implications for protostellar disk

It is proposed that the Balmoral1 parent body formed in close proximity to the ^{16}O-depleted reservoir at large AU. The rarity of ^{16}O-depleted material, and its presence in a CP-IDP, which most likely originated from a comet, also supports the idea that this component formed at large heliocentric distance. As the level of ^{16}O depletion is consistent with that expected from isotope selective self-shielding

(e.g., Yurimoto and Kuramoto, 2004), it is likely that the formation location was also close to that where O self-shielding effects were most pronounced (i.e., the outer solar nebula or even interstellar medium). The ultra-fine-grained/featureless texture of parts of ROI 1 and 2 would be a reasonable fit with this model as silicates formed in the outer solar nebula are expected to be amorphous because this region was too cold to form crystalline materials, and >97% of silicates formed in the ISM are reported to be amorphous (Kemper et al., 2004). The composition of ISM amorphous silicates has been estimated as 84.9% olivine and 15.1% pyroxene, and the grains are thought to be spherical with radii of less than 0.1 μm (Kemper et al., 2004), which is generally in keeping with the grains observed in Balmoral1. It is possible for crystalline silicates to occur in the outer solar nebula but these are more likely to have arrived there by turbulent radial mixing (Bockelée-Morvan et al., 2002) from the inner Solar System.

5. SUMMARY

The results of this study confirm that IDPs are important samples for preserving information about early Solar System reservoirs that are not readily available from, or preserved in, samples originating from asteroids. The IDPs in this study show an extremely wide variation in compositions across single fragments, reflecting the incorporation of a range of different early Solar System reservoirs.

The IDP Lumley reveals that diverse isotopic reservoirs carrying material with distinctive textures that must originate from different settings in the early solar nebula, can be transported and mixed together in the comet-forming region. These materials appear to have been incorporated as micrometre-sized clasts on the Lumley parent body suggesting that they may have been disrupted into smaller clasts from their primary reservoir or location of formation, possibly by collisional events, prior to re-aggregation in the Lumley parent body. These findings are in broad agreement with the model set out in Wozniakiewicz et al. (2012) of pre-accretional sorting of cometary dust.

The IDP Balmoral fragment preserves evidence for the existence of a ^{16}O-depleted reservoir in the early Solar System. It appears that the ^{16}O-depleted material in Balmoral formed directly from the ^{16}O-depleted reservoir itself. Evidence for this reservoir may be rare in the meteorite record either because it is present in parent bodies that formed at large AU and so are not sampled efficiently on Earth, or, that the signature is easily lost through interaction with reservoirs of different compositions during, or after, formation of the parent bodies.

The IDP fragments studied here support models for transport of material from the inner Solar System out to larger heliocentric distances. We hold the view that parent bodies formed at larger heliocentric distance will be expected to have incorporated less inner Solar System material than parent bodies formed at smaller heliocentric distance (e.g., Starkey and Franchi, 2013). However, the new results reveal that the early solar nebula may have formed a number of early reservoirs, from initially primary solar nebula dust condensates, that experienced varied histories (at different times or locations) to produce a diverse range of compositions. These reservoirs, or possibly primary parent bodies, were then disrupted into micrometre-sized clasts and re-incorporated into parent bodies in the comet-forming region where they were also able to incorporate varying degrees of material mixed from the inner Solar System. The IDP Balmoral1 reveals that any models accounting for mixing processes in the early solar nebula must also account for the presence of an extremely ^{16}O-depleted reservoir in the comet-forming region.

ACKNOWLEDGMENTS

The authors would like to thank Diane Johnson for her assistance with preparation of the FIB-section. Gordon Imlach for his assistance with FEG-SEM imaging and Heather Davies for her help with some of the TEM analyses. N.A.S. and I.A.F. were funded by STFC rolling Grant ST/I001964/1. NanoSIMS access was via UKCAN.

APPENDIX A. SUPPLEMENTARY DATA

Supplementary data associated with this article can be found, in the online version, at http://dx.doi.org/10.1016/j.gca.2014.07.011.

REFERENCES

Abe K., Sakamoto N., Krot A. N. and Yurimoto H. (2011) Abundance of cosmic symplectite in Acfer 094 carbonaceous chondrite. *Formation of the First Solar System Solids Conference* #9043 (abstr.).

Abreu N. M. (2013) A unique omphacite amphibole and graphite-bearing clast in Queen Alexandra Range (QUE) 99177: a metamorphosed xenolith in a pristine CR3 chondrite. *Geochim. Cosmochim. Acta* **105**, 56–72.

Aleon J., Engrand C., Robert F. and Chaussidon M. (2001) Clues to the origin of interplanetary dust particles from the isotopic study of their hydrogen-bearing phases. *Geochim. Cosmochim. Acta* **65**, 4399–4412.

Aleon J., Engrand C., Leshin L. A. and McKeegan D. (2009) Oxygen isotopic composition of chondritic interplanetary dust particles: a genetic link between carbonaceous chondrites and comets. *Geochim. Cosmochim. Acta* **73**, 4558–4575.

Alexander C. M. O'D., Fogel M., Yabuta H. and Cody G. D. (2007) The origin and evolution of chondrites recorded in the elemental and isotopic compositions of their macromolecular organic matter. *Geochim. Cosmochim. Acta* **71**, 4380–4403.

Alexander C. M. O'D., Bowden R., Fogel M. L., Herd C. D. K. and Nittler L. R. (2012) The provenances of asteroids and their contributions to the volatile inventories of the terrestrial planets. *Science* **337**, 721–723.

Arpigny C., Jehin E., Manfroid J., Hutsemékers D., Schulz R., Stüwe J. A., Zucconi J. M. and Ilyin I. (2003) Anomalous nitrogen isotope ratio in comets. *Science* **301**, 1522–1524.

Bastien R., Broce S., Brown P., Burkett P. J., Campbell-Brown M., Frank D., Gearheart D., Kapitzke M., Moes T., Rodriguez M., Steel D., Williams T. and Zolensky M. (2013) The 2012 Draconid Storm as observed by the Canadian Meteor Orbit Radar and potentially sampled by ER-2 aircraft. *Lunar Planet. Sci. XXXXIIII*. Lunar Planet. Inst., Houston. #1622 (abstr.).

Bischoff A., Scott E. R. D., Metzler K. and Goodrich C. A. (2006) Nature and origins of meteoritic breccias. In *Meteorites and the*

Early Solar System II (eds. D. Lauretta and McSween). Arizona University Press, pp. 679–712.

Bockelée-Morvan D., Gautier D., Hersant F., Hure J. M. and Robert F. (2002) Turbulent radial mixing in the solar nebula as the source of crystalline silicates in comets. *Astron. Astrophys.* **384**, 1107–1118.

Bockelée-Morvan D., Crovisier J., Mumma M. J. and Weaver H. A. (2005) The composition of cometary volatiles. In *Comets II* (eds. M. Festou, H. U. Keller and H. A. Weaver). Univ. Arizona Press, Tucson, pp. 391–423.

Bockelée-Morvan D., Biver N., Jehin E., Cochran A. L., Wiesemeyer H., Manfroid J., Hutsemekers D., Arpigny C., Boissier J., Cochran W., Colom P., Crovisier J., Milutinovic N., Moreno R., Prochaska J. X., Ramirez I., Schulz R. and Zucconi J. M. (2008) Large excess of heavy nitrogen in both hydrogen cyanide and cyanogen from comet 17P/Holmes. *Astrophys. J.* **679**, L49–L52.

Bradley J. P. (1994) Chemically anomalous preaccretionally irradiated grains in interplanetary dust from comets. *Science* **265**, 925–929.

Bradley J. P. (2003) Interplanetary dust particles. In *Treatise on Geochemistry Meteorites Comets and Planets*, vol. 1 (ed. A. M. Davies). Elsevier, pp. 689–711.

Bridges J. C., Changela H., Nayakshin S., Starkey N. A. and Franchi I. A. (2012) Chondrule fragments from Comet Wild 2: evidence for high temperature processing in the outer solar system. *Earth Planet. Sci. Lett.* **341**, 186–194.

Burbine T. H., McCoy T. J., Meibom A., Gladman B. and Keil K. (2002) Meteoritic parent bodies: their number and identification. In *Asteroids III* (ed. , Jr.W. F. Bottke et al.). Univ. of Arizona, Tucson, pp. 653–667.

Busemann H., Nguyen A. N., Cody G. D., Hoppe P., Kilcoyne A. L. D., Stroud R. M., Zega T. J. and Nittler L. R. (2009) Ultraprimitive interplanetary dust particles from the comet 26P/Grigg–Skjellerup dust stream collection. *Earth Planet. Sci. Lett.* **288**, 44–57.

Ciesla F. J. (2007) Outward transport of high-temperature materials around the midplane of the solar nebula. *Science* **318**, 613–615.

Clayton R. N. (1993) Oxygen isotopes in meteorites. *Annu. Rev. Earth Planet. Sci.* **21**, 115–149.

Clayton R. N. (2002) Self-shielding in the solar nebula. *Nature* **415**, 860–861.

Clayton R. N. and Mayeda T. K. (1999) Oxygen isotope studies of carbonaceous chondrites. *Geochim. Cosmochim. Acta* **63**, 2089–2104.

Davidson J., Busemann H. and Franchi I. A. (2012) A NanoSIMS and Raman spectroscopic comparison of interplanetary dust particles from comet Grogg–Skjellerup and non-Grigg Skjellerup collections. *Meteorit. Planet. Sci.* **47**, 1748–1771.

Engrand C., McKeegan K. D., Leshin L. A., Bradley J. P. and Brownlee D. E. (1999) Oxygen isotopic compositions of interplanetary dust particles: ^{16}O-excess in a GEMS-rich IDP. *Lunar Planet. Sci. XXX*. Lunar Planet. Inst., Houston. #1690 (abstr.).

Floss C., Stadermann F. J., Bradley J. P., Dai Z. R., Bajt S., Graham G. and Lea A. S. (2006) Identification of isotopically primitive interplanetary dust particles: a NanoSIMS isotopic imaging study. *Geochim. Cosmochim. Acta* **70**, 2371–2399.

Floss C., Stadermann F. J., Mertz A. F. and Bernatowicz T. J. (2011) A NanoSIMS and Auger Nanoprobe investigation of an isotopically primitive interplanetary dust particle from the 55P/Tempel–Tuttle targeted stratospheric dust collector. *Meteorit. Planet. Sci.* **45**, 1889–1905.

Fraundorf P. (1981) Interplanetary dust in the transmission electron microscope: diverse materials from the early solar system. *Geochim. Cosmochim. Acta* **45**(915–937), 939–943.

Keller L. P. and Messenger S. (2011) On the origins of GEMS grains. *Geochim. Cosmochim. Acta* **75**, 5336–5365.

Kemper F., Vriend W. J. and Tielens A. G. G. M. (2004) The absence of crystalline silicates in the diffuse interstellar medium. *Astrophys. J.* **609**, 826–837.

Lee M. R. and Smith C. L. (2006) Scanning transmission electron microscopy using a SEM: applications to mineralogy and petrology. *Mineral. Mag.* **70**, 561–572.

Mackinnon I. D. R. and Rietmeijer F. J. M. (1987) Mineralogy of chondritic interplanetary dust particles. *Rev. Geophys.* **25**, 1527–1553.

Matrajt G., Messenger S., Brownlee D. and Joswiak D. (2012) Diverse forms of primordial organic matter identified in interplanetary dust particles. *Meteorit. Planet. Sci.* **47**, 525–549.

McKeegan K. D., Aleon J., Bradley J., Brownlee D., Busemann H., Butterworth A., Chaussidon M., Fallon S., Floss C., Gilmour J., Gounelle M., Graham G., Guan Y., Heck P. R., Hoppe P., Hutcheon I. D., Huth J., Ishii H., Ito M., Jacobsen S. B., Kearsley A., Leshin L. A., Liu M.-C., Lyon I., Marhas K., Marty B., Matrajt G., Meibom A., Messenger S., Mostefaoui S., Mukhopadhyay S., Nakamura-Messenger K., Nittler L., Palma R., Pepin R. O., Papanastassiou D. A., Robert F., Schlutter D., Snead C. J., Stadermann F. J., Stroud R., Tsou P., Westphal A., Young E. D., Ziegler K., Zimmermann L. and Zinner E. (2006) Isotopic compositions of cometary matter returned by stardust. *Science* **314**, 1724–1728.

McKeegan K. D., Kallio A. P. A., Heber V. S., Jarzebinski G., Mao P. H., Coath C. D., Kunihiro T., Wiens R. C., Nordholt J. E., Moses, Jr., R. W., Risenfeld D. B., Jurewicz A. J. G. and Burnett D. S. (2011) The oxygen isotopic composition of the Sun inferred from captured solar wind. *Science* **332**, 1528–1532.

Messenger S. (2000) Identification of molecular-cloud material in interplanetary dust particles. *Nature* **404**, 968–971.

Messenger S. (2002) Opportunities for the stratospheric collection of dust from short period comets. *Meteorit. Planet. Sci.* **37**, 1491–1506.

Messenger S., Keller L. P., Stadermann F. J., Walker R. M. and Zinner E. K. (2003) Samples of stars beyond the solar system: silicate grains in interplanetary dust. *Science* **300**, 105–109.

Mumma M. J. and Charnley S. B. (2012) The chemical composition of comets – emerging taxonomies and natal heritage. *Annu. Rev. Astron. Astrophys.* **49**, 471–524.

Nakamura T., Noguchi T., Tsuchiyama A., Ushikubo T., Kita N. T., Valley J. W., Zolensky M. E., Kakazu Y., Sakamoto K., Mashio E., Uesugi K. and Nakano T. (2008) Chondrule-like objects in short-period comet 81P/Wild 2. *Science* **321**, 1664–1667.

Nakashima D., Ushikubo T., Zolensky M. E. and Kita N. T. (2012) High precision oxygen three-isotope analyses of anhydrous chondritic interplanetary dust particles. *Meteorit. Planet. Sci.* **47**, 197–208.

Nesvorny D., Jenniskens P., Levison H. F., Bottke W. F., Vokrouhlicky D. and Gounelle M. (2010) Cometary origin of the Zodiacal Cloud and carbonaceous micrometeorites. Implications for hot debris disks. *Astrophys. J.* **713**, 816–836.

Nguyen A. N. and Zinner E. (2004) Discovery of ancient silicate stardust in a meteorite. *Science* **303**, 1496–1499.

Nguyen A. N., Busemann H. and Nittler L. R. (2007) Remarkably high abundance of presolar grains in interplanetary dust collected from the comet Grigg–Skjellerup dust stream. *Lunar Planet. Sci. XXXVIII*. Lunar Planet. Inst., Houston. #2332 (abstr.).

Nguyen A. N., Nittler L. R., Stadermann F. J., Stroud R. M. and Alexander C. M. O'D. (2010) Coordinated analyses of presolar grains in the Allan Hills 77307 and Queen Elizabeth Range 99177 meteorites. *Astrophys. J.* **719**, 166–189.

Ogliore R. C., Huss G. R., Nagashima K., Butterworth A. L., Gainsforth Z., Stodolna J., Westphal Joswiak A. J. D. and Tyliszczak T. (2012) Incorporation of a late-forming chondrule into comet Wild 2. *Astrophys. J. Lett.* **745**, L19.

Remusat L., Robert F., Meibom A., Mostefaoui S., Delpoux O., Binet L., Gourier D. and Derenne S. (2009) Proto-planetary disk chemistry recorded by D-rich organic radicals in carbonaceous chondrites. *Astrophys. J.* **698**, 2087–2092.

Robert F. (2006) Solar system deuterium/hydrogen ratio. In *Meteorites and the Early Solar System II*, vol. 943 (eds. D. S. Lauretta and , Jr.H. Y. McSween). University of Arizona Press, Tucson, pp. 341–351.

Sakamoto N., Seto Y., Itoh S., Karamoto K., Fujino K., Nagashima K., Krot A. N. and Yurimoto H. (2007) Remnants of the early Solar System water enriched in heavy oxygen isotopes. *Science* **317**, 231–233.

Seto Y., Sakamoto N., Fujino K., Kaito T., Oikawa T. and Yurimoto H. (2008) Mineralogical characterization of a unique material having heavy oxygen isotope anomaly in matric of the primitive carbonaceous chondrite Acfer 094. *Geochim. Cosmochim. Acta* **72**, 2723–2734.

Shang H., Shu F. H., Lee T. and Glassgold A. E. (2000) Protostellar winds and chondritic meteorites formation of solids: the first step. *Space Sci. Rev.* **92**, 153–176.

Simon S. B., Joswiak D. J., Ishii H. A., Bradley J. P., Chi M. F., Grossman L., Aleon L., Brownlee D. E., Fallon S., Hutcheon I. D., Matrajt G. and McKeegan K. D. (2008) A refractory inclusion returned by Stardust from Comet 81P/Wild 2. *Meteorit. Planet. Sci.* **43**, 1861–1877.

Snead C. J., Keller L. P., Messenger S., McKeegan K. D. and Nakamura-Messenger K. (2012) Mineralogy and oxygen isotope compositions of two C-rich hydrated interplanetary dust particles. *75th Annual Meteoritical Society Meeting*, #5378 (abstr.).

Starkey N. A. and Franchi I. A. (2013) Insight into the silicate and organic reservoirs of the comet forming region. *Geochim. Cosmochim. Acta* **105**, 73–91.

Starkey N. A., Franchi I. A. and Alexander C. O'D. (2013) A Raman spectroscopic study of organic matter in interplanetary dust particles and meteorites using multiple wavelength laser excitation. *Meteorit. Planet. Sci.* **48**, 1800–1822.

Wirick S., Flynn G. J., Keller L. P., Nakamura-Messenger K., Peltzer C., Jacobsen C., Sandford S. and Zolensky M. (2009) Organic matter from comet 81P/Wild2 IDPs and carbonaceous meteorites; similarities and differences. *Meteorit. Planet. Sci.* **44**, 1611–1626.

Wozniakiewicz P. J., Bradley J. P., Ishii H. A., Brownlee D. E., Kearsley A. T., Burchell M. J. and Price M. C. (2012) Grain sorting in cometary dust from the outer solar nebula. *Astrophys. J.* **760**, L23.

Young E. D. and Russell S. S. (1998) Oxygen reservoirs in the early solar nebula inferred from an Allende CAI. *Science* **282**, 452–455.

Yurimoto H. and Kuramoto K. (2004) Molecular cloud origin for the oxygen isotope heterogeneity in the Solar System. *Science* **305**, 1763–1766.

Zolensky M. and Thomas K. L. (1995) Iron and iron-nickel sulphides in chondritic interplanetary dust particles. *Geochim. Cosmochim. Acta* **59**, 4707–4712.

Zolensky M., Zega T. J., Yano H., Wirick S., Westphal A. J., Weisberg M. K., Weber I., Warren J. L., Velbel M. A., Tsuchiyama A., Tsou P., Toppani A., Tomioka N., Tomeoka K., Teslich N., Taheri M., Susini J., Stroud R., Stephan T., Stadermann F. J., Snead C. J., Simon S. B., Simionovici A., See T. H., Robert F., Rietmeijer F. J. M., Rao W., Perronnet M. C., Papanastassiou D. A., Okudaira K., Ohsumi K., Ohnishi I., Nakamura-Messenger K., Nakamura T., Mostefaoui S., Mikouchi T., Meibom A., Matrajt G., Marcus M. A., Leroux H., Lemelle L., Le L., Lanzirotti A., Langenhorst F., Krot A. N., Keller L. P., Kearsley A. T., Joswiak D., Jacob D., Ishii H., Harvey R., Hagiya K., Grossman L., Grossman J. N., Graham G. A., Gounelle M., Gillet Ph., Genge M. J., Flynn G., Ferroir T., Fallon S., Ebel D. S., Dai Z. R., Cordier P., Clark B., Chi M., Butterworth A. L., Brownlee D. E., Bridges J. C., Brennan S., Brearley A., Bradley J. P., Bleuet P., Bland P. A. and Bastien R. (2006) Mineralogy and petrology of comet Wild 2 nucleus samples. *Science* **314**, 1735–1739.

Associate editor: Trevor Ireland